Catalysis Science & Technology

Accepted Manuscript

This article can be cited before page numbers have been issued, to do this please use: A. Mahata, K. S. Rawat, I. Choudhuri and B. Pathak, *Catal. Sci. Technol.*, 2016, DOI: 10.1039/C6CY01709F.

ROYAL SOCIETY OF CHEMISTRY

www.rsc.org/catalysis

Cuboctahedral vs. Octahedral Platinum Nanoclusters: Insights into the Shape-dependent Catalytic Activity for Fuel Cell

Arup Mahata,[†] Kuber Singh Rawat,[†] Indrani Choudhuri,[†] Biswarup Pathak, [†,#,*]

[†]Discipline of Chemistry, School of Basic Sciences, Indian Institute of Technology (IIT) Indore, Indore, M.P., India
[#]Discipline of Metallurgy Engineering and Material Science, Indian Institute of Technology (IIT) Indore, Indore, M. P., India
Email: biswarup@iiti.ac.in

Abstract:

The shape of a catalyst plays an important role toward any catalytic reactions. The shape-dependent catalytic activities of two platinum nanoclusters (NCs) with cuboctahedral (Pt_{79}) and octahedral (Pt_{85}) shapes have been investigated toward oxygen reduction reaction (ORR). Energetic stability, thermal stability and dissolution limit of the NCs investigated for their synthesis and practical usages. The four-electron (H_2O formation) vs. two-electron (H_2O_2 formation) ORR mechanisms are systematically studied on the (111) facet of the NCs to get more insights into the shape dependent ORR activity and product selectivity (H_2O vs. H_2O_2). Thermodynamic (reaction free energies) and kinetic (free energy barriers, and temperature dependent reaction rates) parameters are investigated to find out the most favored ORR pathway and product selectivity. The NCs based Pt catalysts are very efficient and selective with respect to the previously reported bulk metal (Pt, Pd, and Ag) based catalysts. Our results show that the rate-determining step is no longer a rate-determining step when the reaction is catalyzed by the cuboctahderal NC. The excellent catalytic activity of the cuboctahedral NC is credited to the surface energy, compressive strain and d-band center position of the catalyst. Our results are very much consistent with experimental findings, and thereby such NCs based electrodes may serve as good candidates for fuel cell applications.

Keywords: Heterogeneous Catalysis, Shape-dependent Catalytic Activity, Oxygen Reduction Reaction, Fuel Cell

1. Introduction

Proton exchange membrane (PEM) fuel cells are one of the most promising devices for clean energy due to their high efficiency, low operating temperature and zero emission.[1-4] ORR is the key reaction at the cathode, which controls the performance of a fuel cell. However, the slow reaction kinetics associated with the ORR remains one of the major limitations for commercialization of low-temperature fuel cells.[5-6] Besides, the high Pt loading in a state-of-the-art ORR electrocatalyst is also a topic of major concern.[7] These can be addressed either by reducing the Pt-loading of the catalyst or by changing the morphology of the platinum catalyst. In order to lower the Pt-loading, alloying Pt with other transition metals has been emerged as a good alternative for efficiency and stability of the catalyst. Such alloying with other metals leads to the formation of bi-metallic,[8-10] mixed alloy[11-12] and core-shell structures.[13-15] However, due to the dissolution of surface atoms and leaching of the active metal[16], the durability of these catalysts is far from the scenario of commercialization. On the other hand, the catalytic activity of the Pt-based catalysts can be improved by changing the morphology; designing nanoparticles with desirable shapes. Apart from the different metal-based catalysts, the shape of the metal nanoparticle plays a very important role to maximize the specific activity of the catalyst.[17] Therefore, the shape-controlled synthesis of a nanocrystal with exposed active surface sites is a topic of current interest.

El-Sayad and co-workers[18] have given the breakthrough by synthesizing a series of shape-controlled colloidal platinum nanoparticles in the shapes of tetrahedral, cubic, irregular-prismatic, icosahedral and cuboctahedral structures. Later on, extensive studies have been

performed for the synthesis of shape-controlled well-defined platinum nanocatalysts[19-24]. Sun and co-workers[19] have developed a very facile shape-controlled synthesis technique for platinum nanoparticles and they established a major effect on the ORR of the PEM fuel cell. Using the scanning electrochemical microscopy, Carlos et al.[20] reported that the hexagonal platinum nanoparticle with (111) and (100) facets exhibits an enhanced ORR activity while comparing with the spherical and cubic nanoparticles. The shape-controlled synthesis of the Pt_3Ni nanoctahedra terminated with (111) facets improves the ORR activity by five-fold compared to the similar sized Pt_3Ni nanocube terminated with (100) facets.[21] Over the past few years, considerable progresses have been made on the area of shape-controlled synthesis as well as shape-dependent activity of platinum nanoparticles for ORR activity.[25-29] The shape of the catalyst is also very important for improving the product selectivity as reported for many organic reactions such as benzene hydrogenation[30], pyrrole hydrogenation[31], butene isomerization[32], glucose oxidation[33], formic acid oxidation[34], and CO oxidation[35] reactions.

Despite the extensive experimental studies on the shape-dependent activity, there is a lack of understanding about the dissimilar catalytic activities of different shaped NCs toward a particular reaction. To the best of our knowledge, there are no reports on the ORR reduction on a well-defined NC-based catalyst. Therefore, it is necessary to model NCs of different shapes surrounded by well-defined facets to understand their catalytic activities toward ORR. Here, we have modeled two NCs of similar size in the shapes of cuboctahedral (Pt_{79}) and octahedral (Pt_{85}) geometries and surrounded by well-defined facets. The cuboctahedral and octahedral NCs (Figure 1) are considered for our study as these shapes are often realized experimentally.[36,37] Besides, Pt(111) and Pt(100) are the highly exposed surfaces in the experimentally synthesized Pt-nanoclusters.[38]

ORR involves many-electron reduction reaction and it can proceed either through a more efficient four-step, four-electron reduction with the formation of H_2O or via a two-step, two-

electron reduction for the formation of H_2O_2.[39] However, the four-electron reduction ($4e^-$) is preferred over two-electron ($2e^-$) reduction in order to maximize the efficiency. Besides, H_2O_2 formation affects the durability of the membrane of a PEM fuel cell.[40] Thereby, the product selectivity (H_2O vs. H_2O_2) is very important for the performance of a fuel cell. Therefore, a systematic study based on the reaction free energy and activation barriers of all the possible elementary steps is done to understand the shape dependent catalytic properties of the NCs. For comparisons, our results are compared with the available theoretical and experimental data on the bulk Pt(111) surface. Kinetic analysis is performed to gain more insights into the rate of reaction and product selectivity (H_2O vs. H_2O_2). Therefore, in the present investigation, we have demonstrated an atomic level understanding toward the shape-dependent catalyst durability, catalytic activity, and product selectivity of the platinum nanocatalysts toward ORR. This study will certainly provide a significant insight into the designing of an efficient catalyst for fuel cell applications.

2. Model and Computational Details

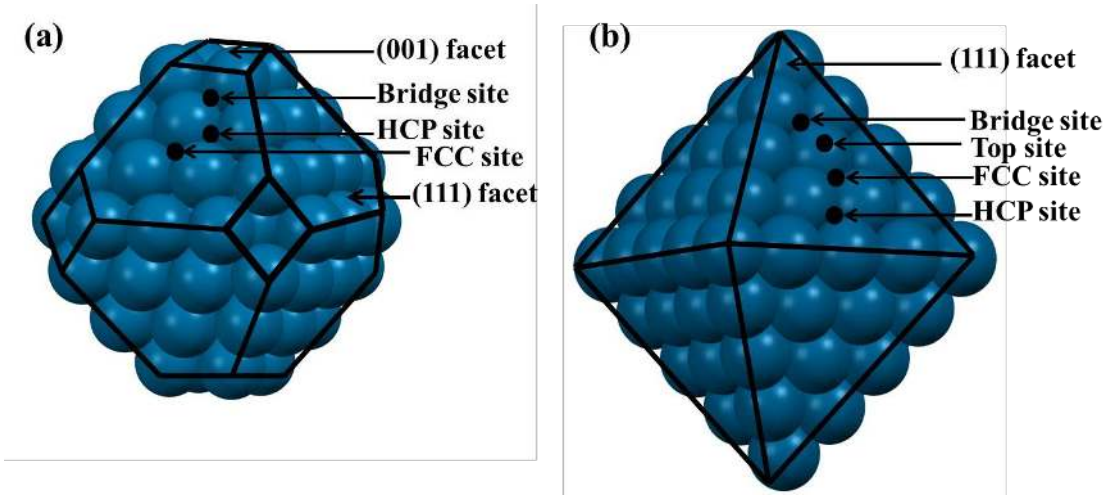

Figure 1: (a) Cuboctahedral NC (Pt_{79}) with eight (111) and six (001) facets and (b) Octahedral NC (Pt_{85}) with eight (111) facets.

Cuboctahedral and octahedral Pt NCs are synthesized with majorly exposed (111), (002) and/or (200) facets[38]. Therefore, we have modeled two NCs of ~1.5 nm in the shape of cuboctahedral (Pt_{79}) and octahedral (Pt_{85}) geometry. The cuboctahedral Pt_{79} NC (Fig. 1a) is modeled with eight (111) and six (001) facets, whereas the octahedral Pt_{85} NC (Fig. 1b) is modeled with eight (111) facets. Previous experimental and theoretical reports show that Pt(111) surface shows better ORR activity than Pt(100) or any other Pt-surfaces[9,41]. In fact the specific activity of Pt(111) surface reported to be two times higher than the Pt(100) surface.[9] Further, the sequence of ORR activity on Pt surface reported to be in the following order: (100) < (110) < (111).[41a,e-f] More importantly, the ORR activity is highest even on the (111) facet of Pt alloy based catalysts.[41b-d] Therefore, inspired by all these findings, we have chosen the (111) facet for studying ORR reaction mechanism.

The first-principles calculations are performed using a projector augmented wave (PAW)[42] method as implemented in the Vienna Ab initio Simulation Package (VASP).[43] The exchange-correlation potential is described by using the generalized gradient approximation of Perdew-Burke-Ernzerhof (GGA-PBE).[44] The PAW method is employed to treat interactions between ion cores and valance electrons.[42] Plane wave with a kinetic energy cut off of 470 eV is used to expand the electronic wave functions. A 25 × 25 × 25 $Å^3$ cubic supercell is used to optimize the metal clusters to rule out the possibility of interactions between the periodically repeated metal clusters. The Brillouin zone is sampled with a Gamma point (1×1×1) for clusters. The total energy of the Pt_{79} and Pt_{85} cluster are improved by 0.001 and 0.002 eV, respectively if the k-point mesh set to 2 × 2 × 2. Therefore, we have used Gamma point for all the calculations to save the computational cost. All the atoms are relaxed for the full structural relaxation. The bulk Pt(111) is modeled with a (2 × 2) supercell to minimize the lateral interactions between the repeating images. The metal slab is composed of five atomic layers, where the bottom three layers are fixed and the top two

layers are relaxed. A 12 Å of vacuum is used along the z-direction to avoid any periodic interactions. The Brillouin zone is sampled using a 3 × 3 × 1 k-point grid for the surface calculations. All the systems are fully optimized, where the convergence criteria for total energy and forces are set at 10^{-4} eV and <0.02 eV/Å, respectively. Spin-polarized calculations are performed for all the molecular species and oxygen adsorbed intermediates. We have included Grimme's D3-type[45] of semiempirical method to include the dispersion energy corrections for van der Walls interactions. The climbing nudged elastic band (CI-NEB) method[46] is used to locate the transition state. Six intermediate images are used in each CI-NEB pathway. Vibrational frequencies for the initial, transition and final states of the reaction are calculated and the transition states are confirmed by the presence of one imaginary frequency. Zero-point energy (ZPE) is calculated using the following equation:

$$\text{ZPE} = \sum_i 1/2h\upsilon_i$$

where h is the Planck constant and υ_i is the frequency of the i^{th} vibrational mode. In this work, we employ same methodologies for the energies (free energy and adsorption energy) and activation barrier calculations as in reference 41g-h.

3. Results and Discussion

We have divided this section into three parts. In the first part, we have investigated the energetic stability, thermal stability, dissolution nature, and coalescence behavior of the NCs. Then, the adsorption behaviors of the ORR intermediates on the (111) facet of the NCs are studied and compared with previous theoretical and experimental reports over the bulk Pt(111) surfaces. The catalytic activities are compared with the previously reported bulk Pt(111) based catalysts, as there are no reports (on full ORR mechanism) on a well-defined platinum NC. Furthermore, all possible ORR mechanisms are studied followed by an attempt is made to find out the role of the shape toward the ORR activity. Finally, kinetic analysis has

View Article Online
DOI: 10.1039/C6CY01709F

been performed to explore the efficiency and selectivity of the NCs toward four-electron vs. two-electron reduction.

3.1 Stability of the NCs:

The stability of the NCs is very important for their synthesis and practical usages. Cohesive and formation energy calculations are performed to evaluate the thermodynamic stability of the NCs. For comparisons, we have calculated cohesive energies for the bulk Pt(111) and face centered cubic (fcc) Pt. The calculated cohesive energies are -4.87, -4.91, -5.47 and -5.71 eV/atom for the cuboctahedral, octahedral, bulk Pt(111) and fcc platinum structures, respectively. Our calculated cohesive energy value of the bulk platinum is very much in agreement with the experimental value of -5.84 eV/atom.[47] Further, the formation energies[48-49] are calculated and the calculated formation energies are 0.82, 0.78 and 0.23 eV/atom for the cuboctahedral, octahedral and bulk Pt(111) respectively. The negative cohesive energy values indicate that the NCs are thermodynamically stable and the formation energy values predict that the NCs are separated by low energy differences.

The thermal stability of the NCs is verified by carrying out Ab Initio Molecular Dynamics Simulations (AIMD) using canonical ensemble at 300-500 K with a time step of 1 femtosecond. Temperature control is achieved by nose thermostat model.[50] First, the structure is heated at 300 K with a time step of 1 femtosecond (fs) for 20 picoseconds (ps). In case of cuboctahedral NC, no structure reconstruction is found after the simulation, whereas the edge atoms are moving inwards for the octahedral NC. We have carefully investigated the structure of the NCs during the AIMD simulation at 300 K. We find that the diameter of the cuboctahedral (11.31 Å) decreases to 11.16 Å and the diameter of the octahedral (14.85 Å) NC decreases to 14.54 Å. The fluctuation of the total energy of cuboctahedral NC is smooth throughout the AIMD simulations (Figure 2a). Hence, the structure remains stable at room

View Article Online
DOI: 10.1039/C6CY01709F

temperature. In contrary, the fluctuation of total energy is very high for octahedral NC (Figure 2c). Therefore, the total energy fluctuation can be related to the changes in the diameter of the NCs. Further, simulations using an NVT ensemble at 400 and 500 K with a time step of 1 fs are carried for 20 ps. We have plotted the root mean square displacement (RMSD) as a function of time step (Figure 2b and 2d) for all the cases. Our RMSD plots show that atomic displacements of cuboctahedral are negligible throughout the temperature ranges (300-500 K). The snapshots of atomic configurations of NCs at the end of MD simulations are shown in Supporting Information. We did not find any structural reconstruction of cuboctahedral NC (see Figure S1 of Supporting Information for details) even after heating at 500 K for 20 ps. These results demonstrate that the NCs are separated by high-energy barriers from other local minima structures and they are stable in the fuel cell operating temperatures.

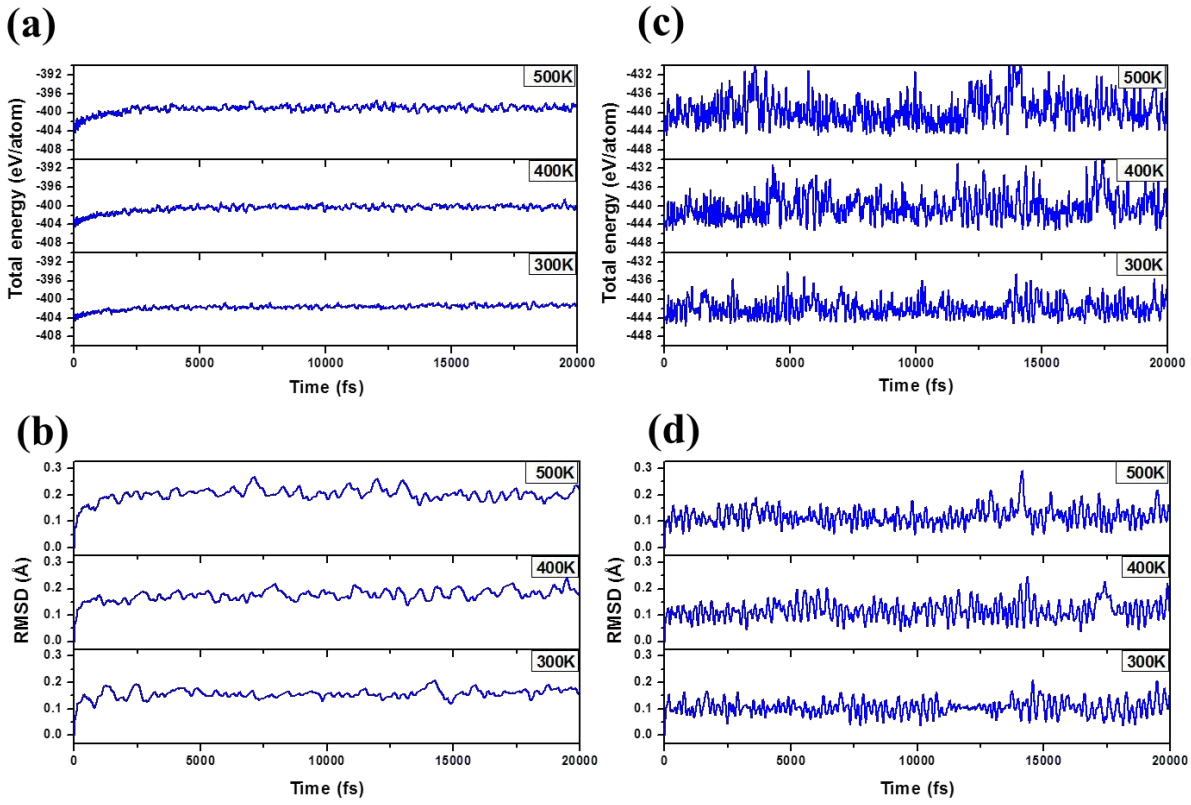

Figure 2: Molecular dynamics simulation analysis at different temperatures as a function of time step: (a-b) Cuboctahedral NC and (c-d) Octahedral NC.

View Article Online
DOI: 10.1039/C6CY01709F

Apart from the energetic and thermal stability of the NC, the dissolution of surface atoms of the nanoparticle is also a very important criterion to describe the electrochemical stability of the catalyst.[51-52] Catalysts of different shapes are different in terms of the extent of unsaturation and hence toward dissolution. Therefore, nanoparticles with different shapes possess different extent of resistant toward dissolution in a fuel cell. It is well accepted that the electrochemical oxidation of Pt ($Pt \rightarrow Pt^{2+} + 2e^-$) is the main phenomenon behind the dissolution.[53-55] We have compared the dissolution behavior of the NCs with respect to the bulk Pt(111). As the surrounding environment i.e. the presence of oxygen largely influences the dissolution, the calculations are carried out in the presence of O-atom (see Text S2 of Supporting Information for details). Such model has been used for calculating the shift in dissolution potential.[51,53-55] Here, the shift (ΔU) in the electrode potential is calculated with respect to bulk Pt(111) using the following equation:

$$\Delta U = U_{NC} - U_{Pt(111)} = (\mu_{Pt-Pt(111)} - \mu_{Pt-NC})/(ne)$$

where U_{NC}, $U_{Pt(111)}$, $\mu_{Pt\text{-}NC}$, $\mu_{Pt\text{-}Pt(111)}$ and n are the electrode potential of the NC, electrode potential of the bulk Pt(111), chemical potential of platinum metal of the NC, chemical potential of platinum metal of the bulk Pt(111) and number of electron transferred during the dissolution reaction ($Pt \rightarrow Pt^{2+} + 2e^-$), respectively (see Text S2 of Supporting Information for details). The negative ΔU value for NC represents that the dissolution of the NC is faster than the bulk Pt(111).

View Article Online
DOI: 10.1039/C6CY01709F

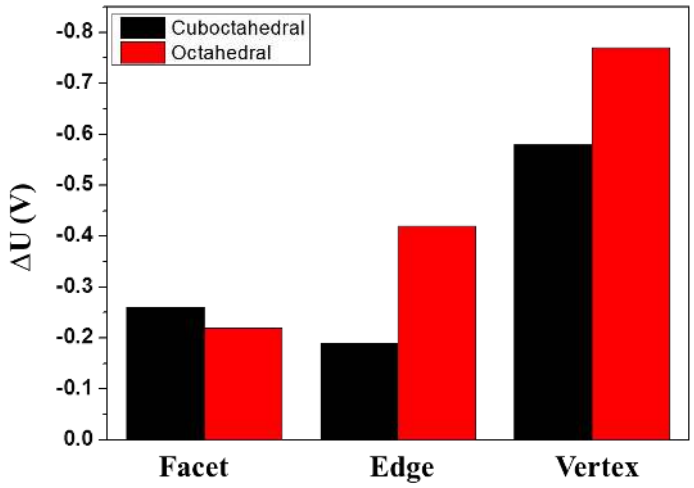

Figure 3: The shift in electrode potential of the atoms of the NCs at different sites (facet, edge and vertex) with respect to the bulk Pt(111) in the O environment.

We have calculated the shift in the electrode potential of the facet, edge and vertex atoms of the NCs (see Figure S3-S5 of Supporting Information for their atomic structures). Our results show that the vertex atoms are most prone to dissolution, followed by edge and facet atoms for both the NCs (Figure 3). Vertex atoms possess highest unsaturation that causes them to dissolve fast. We find that the facet atoms of the octahedral NC are more stable than that of the cuboctahedral one from dissolution. Interestingly, edge and vertex atoms of the cuboctahedral NC are more stable than the edge and vertex atoms of the octahedral NC. Moreover, we have calculated the dissolution potential in the presence of *OH and *OOH. Our results (Figure S6 & S7; Supporting Information) show that the extent of dissolution is highest in the oxygen environment and least in the OOH environment. This is due to the strong adsorption nature of *O, which destabilizes the NC more than when *OOH is adsorbed. However, the trend of the shift of dissolution potential is similar for vertex, edge and facet sites irrespective of the reaction environment. Therefore, the electrochemical stability of the cuboctahedral structure is better than the octahedral one. Hiroaki et al.[56] concluded that the dissolution of the nanoparticle starts from the terrace atoms instead of

edge atoms of a cubic platinum nanoparticle. Recently, Ruttala et al.[57] found that the Pt-cuboctahedra is more stable than the Pt-nanocube due to the higher dissolution rate of the (100) facet than the (111) facet. Therefore our results are very much in consistent with previous reports.

3.2 ORR Mechanism

3.2.1 Adsorption

Four different catalytic sites (Figure 1) are present on the Pt(111) facet of the NCs: (i) top, (ii) bridge, (iii) face centered cubic (fcc) and (iv) hexagonal close packed (hcp). The most preferred binding sites of the intermediate species and their respective binding energies are given in Table 1. For comparison, we have calculated adsorption energies of the intermediate species on the bulk Pt(111). We find that the preferred binding sites are same for all the adsorbates on the NCs and bulk Pt(111). It is interesting to find that the $*O_2$ and *O bind very strongly on the (111) facet of the NCs than on the bulk Pt(111), whereas the hydrogenated intermediates (*OH and *OOH) and products ($*H_2O$ and $*H_2O_2$) have comparable binding energy on the NCs and bulk Pt(111). Moreover, $*O_2$, *O and *OH bind very strongly on the cuboctahral NC surface than on the octahedral NC. However, the adsorption energy of $*H_2O$ and $*H_2O_2$ are comparable on both the NCs. A detailed discussion of the adsorption behaviors of the intermediates and comparison with the previous experimental and theoretical data has been given in the Supporting Information (Figure S2 and Text S1). Furthermore to take into account the adsorption behaviour at the low-coordinated site, we have calculated the adsorption energies of all the possible reaction species at the edge site of the NCs and the values have been provided at the Supporting Information (Table S1, Supporting Information). It is very interesting to note that all the species except *O bind strongly on the edge position

compared to the facet. The strong adsorption energy of the end products (*H_2O and *H_2O_2) poisons the catalyst surface.

Table 1: Preferred binding sites, binding energies (eV) of the most stable ORR intermediate species on the (111) facet of the NCs and bulk Pt(111) surface. Here t, b, h and f denote top, bridge, hcp, and fcc sites, respectively.

Adsorbed Species	Octahedral (Pt_{85})	Cuboctaheral (Pt_{79})	Pt(111)
*O_2	-1.43 (b)	-1.56 (b)	-0.79 (b)
*O	-4.90 (f)	-5.19 (f)	-4.54 (f)
*OH	-2.38 (t)	-2.49 (t)	-2.40 (t)
*OOH	-1.38 (b)	-1.40 (b)	-1.22 (b)
*H_2O_2	-0.31 (b)	-0.34 (b)	-0.34 (b)
*H_2O	-0.21 (t)	-0.23 (t)	-0.26 (t)
*H	-2.76 (f)	-2.80 (f)	-2.80 (f)

3.2.2 Reaction Mechanism

During ORR, H_2O and H_2O_2 are the two end products, which are formed via four-electron ($4e^-$) and two-electron ($2e^-$) reduction reactions, respectively. We have considered two important pathways for O_2 dissociation: (i) direct and (ii) indirect pathways.[41g-h] In case of direct pathway, O-O bond dissociation is favored over hydrogenation, whereas in case of indirect pathway, hydrogenation is preferred over O-O bond dissociation.[41g-h] Further, the product selectivity (H_2O vs. H_2O_2) can be related to the direct vs. indirect mechanism.

View Article Online
DOI: 10.1039/C6CY01709F

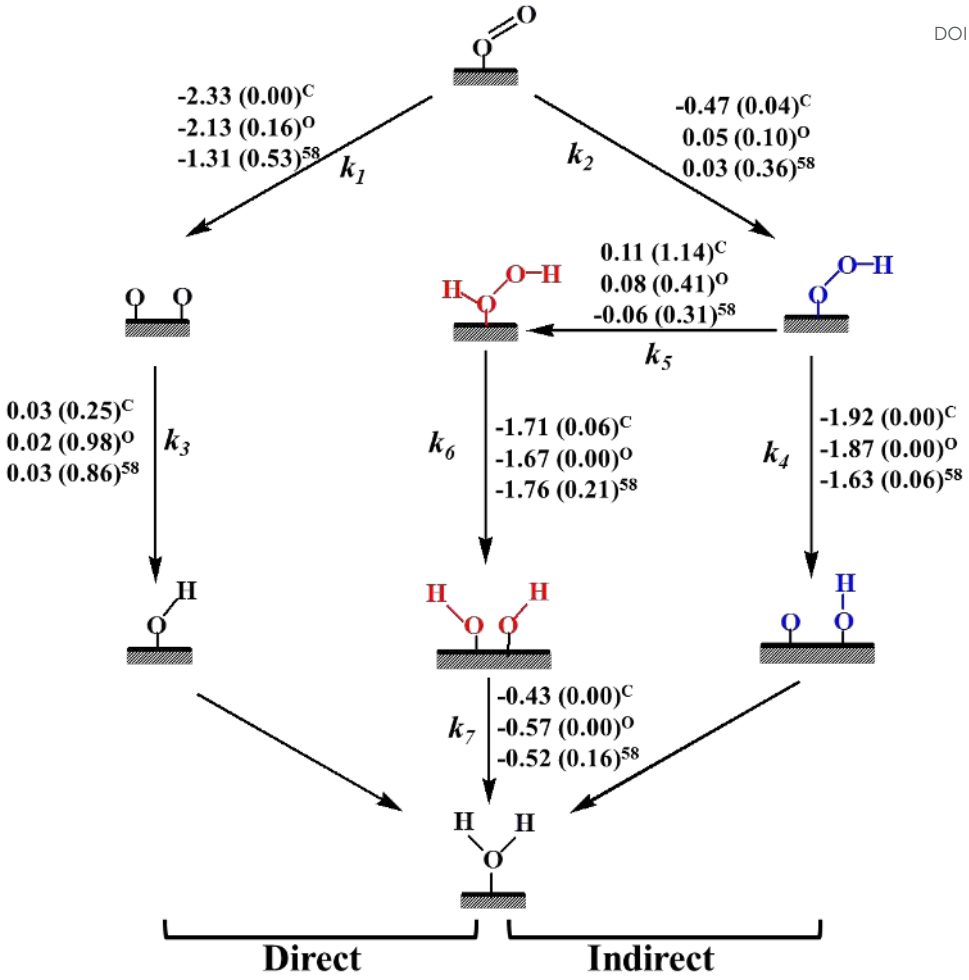

Scheme 1: Reaction free energies (eV) and activation barriers (eV, in parenthesis) are presented for all the possible elementary steps of ORR over (111) facet of the NCs, where C and O represent for the cuboctahedral and octahedral NCs, respectively. Our calculated respective values are compared with the previous reports on the bulk Pt(111).[58]

O_2 activation:

Direct O-O bond dissociation via $4e^-$ reduction is a very important step for the fuel cell applications as it leads to the formation of H_2O. Moreover, direct dissociation reduces the possibility of unwanted by-products formation. Previous studies on bulk metal surfaces (Pt, Pd and Ag) show that direct O-O bond dissociation (step 1) is not kinetically favored over

hydrogenation (step 2).[59-60] Thus, the $*O_2$ can be dissociated into atomic oxygen (*O) or can be hydrogenated to *OOH.

Table 2: Reaction free energies (ΔG in eV) and activation barriers ($\Delta G^{\ddagger}$ in eV) for the all-possible elementary reactions on the (111) facet of the cuboctahedral and octahedral NCs.

Steps	Elementary Reactions	Cuboctahedral		Octahedral	
		ΔG	$\Delta G^{\ddagger}$	ΔG	$\Delta G^{\ddagger}$
1	$*O_2 \rightarrow *O + *O$	-2.33	0.00	-2.13	0.16
2	$*O_2 + *H \rightarrow *OOH$	-0.47	0.04	0.05	0.10
3	$*O + *H \rightarrow *OH$	0.03	0.25	0.02	0.98
4	$*OOH \rightarrow *O + *OH$	-1.92	0.00	-1.87	0.00
5	$*OOH + *H \rightarrow *H_2O_2$	0.11	1.14	0.08	0.41
6	$*H_2O_2 \rightarrow *OH + *OH$	-1.71	0.06	-1.67	0.00
7	$*OH + *H \rightarrow *H_2O$	-0.43	0.00	-0.57	0.00

The direct $*O_2$ bond dissociation is a barrierless process with reaction free energy of -2.33 eV on the (111) facet of the cuboctahedral NC. However, the activation barrier is 0.16 eV with a reaction free energy of -2.13 eV on the (111) facet of the octahedral NC. Paul et al.[61] also reported that the O-O bond dissociation is a barrierless process over the Pt_{79} NC. The previously calculated O-O bond dissociation barriers are 0.53 eV[58], 0.45 eV[61] and 0.44 eV[59] on the bulk Pt(111); 0.72 eV and 1.22 eV on the bulk Pd(111)[59] and Ag(111)[60] surfaces, respectively. Therefore, the NCs show superior activity towards direct O_2 dissociation over the bulk surfaces. Moreover, the octahedral NC requires 0.16 eV of more energy for the direct O-O dissociation than the cuboctahedral NC. Therefore, the shape of the catalyst influences the activation of O-O bond. In fact, the *O-O bond distances in the cuboctahedral

View Article Online
DOI: 10.1039/C6CY01709F

and octahedral NCs are 1.29 and 1.27 Å, which indicate that the activation of $*O_2$ is favored on the cuboctahedral (111) facet. The vibrational frequencies of the *O-O bond while adsorbed on the cuboctahedral and octahedral facets are 1200 and 1266 cm^{-1}, respectively, which also support our finding.

Similarly, O_2 hydrogenation (step 2) on the cuboctahedral NC is exergonic (-0.47 eV) with an activation barrier of 0.04 eV, whereas the O_2 hydrogenation is an uphill process (0.05 eV) with an activation barrier of 0.10 eV on the octahedral NC. The previous reported barriers for O_2 hydrogenation (step 2) are 0.25[63], 0.36[58] and 0.30 eV[59] on the bulk Pt(111).

Interestingly, we find that the direct O_2 bond dissociation is slightly favorable (thermodynamically and kinetically) on the (111) facet of the cuboctahedral NC over the O_2 hydrogenation step. However, the octahedral NC shows a different catalytic trend, though both the steps (steps 1-2) are very much comparable. Previous studies reported that O_2 hydrogenation is more favorable over direct O_2 bond dissociation on the Pt(111), Pd(111) and Ag(111) surfaces. Therefore, the octahedral NC shows a similar trend in ORR activity like other bulk (111) surfaces. Moreover, the octahedral NC favors *OOH formation, which increases the possibility of H_2O_2 formation.

***OH formation:**

The *OH formation is another important step for ORR and this step is reported to be a rate determining step of ORR on bulk Pt(111). [58-59,62] The direct O-O bond dissociation leads to the formation of *O, which subsequently undergoes hydrogenation for the formation of *OH (step 3). The formation of *OH (step 3) on the octahedral NC is slightly endergonic (0.02 eV) with an activation barrier of 0.98 eV. However, the *OH formation step requires a lower activation barrier (0.25 eV) on the cuboctahedral NC. Previous studies reported activation barriers of 0.74[59] and 0.86 eV[58] on the bulk Pt(111) and 0.72 eV on the Pd(111) surfaces.[60]

View Article Online
DOI: 10.1039/C6CY01709F

Therefore, the *OH formation is very much favorable on the cuboctahedral NC surface than on the octahedral NC and bulk Pt(111) surfaces. The lower barrier for the *OH formation on the cuboctahedral NC surface is might be due to the strong adsorption of *OH on the cuboctahedral NC surface (-2.49 eV) than on the octahedral NC surface (-2.38 eV). Moreover, we have carefully investigated the energetics and structural parameters of the transition state to provide the clear understanding behind the distinct nature of *OH formation on the NCs. The Pt-Pt distance is similar (2.67 Å) in both the bare NCs. However, the structural parameters are different in their respective *OH formation transition states (TS). On the cubooctahedral NC, the transition state structure for *OH formation is close to the product structure, whereas the corresponding structure is close to the reactant on the octahedral NC. As *O adsorbs strongly compared to *OH, therefore the extent of deformation on the (111) facet of the NCs are different in their respective transition states. The Pt-Pt bond distances are 2.77 and 2.93 Å on the cuboctahedral and octahedral NC, respectively. Therefore, octahedral NC is under highly strained (9.7%), which makes the TS less stable compared to the transition state on the cuboctahedral NC (3.7% strained). Moreover, we have calculated the strain energy of the NCs in their respective TS geometry. The strain energy of the TS is calculated by evaluating the energy difference between the optimized NC and the single-point energy of the NC within the geometry of the transition states. Our calculated strain energies are 0.73 and 0.26 eV for the octahedral and cuboctahedral NC, respectively. Therefore, the product like transition state makes the *OH formation favorable on the cuboctahedral NC. This may be due to the presence of two different facets (111) and (100) in the cuboctahedral NC.

We have also calculated the activation barriers for *OH formation (*O + *H → *OH) step at the edge site. The calculated activation barriers for the *OH formation are 1.24 and 0.63 eV on the cuboctahedral and octahedral NCs, respectively. Thereby, *OH formation is

View Article Online
DOI: 10.1039/C6CY01709F

favourable on the (111) facet than at the edge site of cuboctahedral NC and the trend is opposite on the octahedral NC. The anomaly can be explained from the adsorption energy of the *O and *OH on the NCs. Octahedral NC binds *O in almost similar way on the edge (-4.80 eV) and facet (-4.90 eV) sites, whereas cuboctahedral NC binds weakly (by 0.30 eV) at the edge site compared to facet site. Therefore, the charge transfer from the cuboctahedral NC towards *O will be less at the edge site, which hinders the protonation step.

The site dependent catalytic activity has been reported previously. Gao et al.[64a] showed some interesting findings on site specific reactivity of Pd nanoparticles for CO2 reduction and hydrogen evaluation reaction (HER) and reported that the corner, edge, and terrace sites are active for HER, whereas edge sites are active for CO_2 reduction. Using DFT and microkinetic modeling, Cai et al.[64b] investigated the site specific reactivity on furfural conversion over platinum (Pt) catalysts and reported that the reaction pathways in furfural conversion (hydrogenation or decarbonylation) largely depend strongly on the reactive sites of the catalysts. Furthermore, Lyu et al.[64c] also reported that the hydrodehalogenation of nitrobenzene highly dependent on the type of reaction sites, whereas the hydrogenation pathways show almost similar activity on different reaction sites.

Furthermore, *OH formation is possible via indirect pathways (step 4) too; such as via peroxyl formation followed by O-O bond dissociation (step 4). This step is a barrierless process on both the NCs with reaction free energies of -1.92 and -1.87 eV for the cuboctahedral and octahedral NCs, respectively. Yao *et al.*[59] and Kai *et al.*[58] reported activation barriers of 0.12 eV and 0.06 eV, respectively for the *OOH dissociation (step 4) step over the bulk Pt(111). Therefore, the *OOH dissociation in general is a favorable process over the NCs and bulk surfaces.

View Article Online
DOI: 10.1039/C6CY01709F

***H_2O_2 Formation and Decomposition:**

The $2e^-$ reduction process leads to the formation of H_2O_2. H_2O_2 can be formed (step 5) via two successive hydrogenations on O_2 ($*O_2 + *H \rightarrow *OOH$, $*OOH + *H \rightarrow *H_2O_2$). Our calculated activation barrier and reaction free energy for H_2O_2 formation are 0.41 and 0.08 eV, respectively over the octahedral NC surface. In fact, the cuboctahedral NC requires far higher activation energy than the octahedral NC for the formation of H_2O_2. Zhiyao *et al.*[63] reported an activation barrier of 0.19 eV for the H_2O_2 formation (step 5) on the bulk Pt(111). This suggests that H_2O_2 formation is favorable on bulk Pt(111), whereas it is not favorable on the cuboctahedral NC surface. The dissociation of $*H_2O_2$ into *OH (step 6) is very much comparable on both the NCs. The activation barriers for $*H_2O_2$ dissociation steps (step 6) is a barrierless process on the octahedral NC, whereas it shows an activation barrier of 0.06 on the cuboctahedral NC.

***H_2O formation:**

The adsorbed *OH undergoes further hydrogenation (step 7) towards the formation of $*H_2O$. This is calculated to be a barrierless process on the NCs surface. The previous studies reported H_2O formation barriers of 0.16 eV,[60] and 0.14 eV[59] on the bulk Pt(111), which are higher than our calculated barriers on the NCs surface. However, the $*H_2O$ formation is favorable over *OH formation on the surface of the NCs. This suggests that the *OH formation is the rate determining step on the NCs and $*H_2O$ formation will not influence the reaction kinetics on the NC facet. We find that the $*O_2$ dissociation ($*O_2 \rightarrow *O + *O$) and *OH formation ($*O + *H \rightarrow *OH$) steps are significantly improved over the cuboctahedral NC surface than on the octahedral NC surface. Therefore, our results show that the shape of the NCs has a significant role on the ORR activity. Moreover, the shape is not only

View Article Online
DOI: 10.1039/C6CY01709F

influencing the rate-determining step (step 3) but also other important steps. So if we compare the catalytic activity of the cuboctahedral and octahedral NCs toward ORR then we find that the cuboctahedral NC is highly selective for four-electron reduction over two-electron reduction. Thus, we predict that the cuboctahedral NC could be a promising catalyst for fuel cell applications.

3.2.3. Origin of the Reactivity:

We have calculated the surface energies of the NCs to understand the excellent catalytic activities of the NCs with respect to the bulk Pt(111). The calculated surface energies for the cuboctahedral NC, octahedral NC and bulk Pt(111) are 0.176, 0.172, and 0.114 eV/Å^2, respectively. The presence of low coordinated sites is the reason for high surface energy of the NCs. Thus, our results indicate that the NCs are highly reactive compared to the bulk Pt(111) and the cuboctahedral NC is the most active one, which is very much consistent with our ORR activity study.

Furthermore, we have calculated the strain energy on the facet of the NCs to understand the excellent catalytic activity of the cuboctahedral NC (see Text S4 of Supporting Information for details). The calculated strain energies for the cuboctahedral and octahedral NCs are -4.58 and -6.55 eV, respectively. Therefore, the cuboctahedral NC is more reactive than that of octahedral NC. We have carefully investigated the geometrical parameters of the NCs to find out the origin of such reactivity. The average Pt-Pt bond distances of the facet atoms are 2.66 Å for both the cuboctahedral and octahedral NCs compared to 2.77 Å in the bulk Pt(111). Surprisingly, the Pt-Pt bond distances of the edge atoms are 2.64 and 2.62 Å for the cuboctahedral and octahedral NCs, respectively. However, the Pt-Pt bond distance of the (100) facet of the cuboctahedral NC is 2.71 Å. Therefore, due to the presence of two different

View Article Online
DOI: 10.1039/C6CY01709F

facets in the cubocatahedral structure, the surface is under strain, which in turn improves the catalytic activity.

We have further calculated the % of strain on the cuboctahedral and octahedral NCs and our results show that the cuboctahedral NC is under less compressive strain (more tensile strain) than the octahedral NC (see Text S4 of Supporting Information for details). Besides, the d-band center of the (111) facet of both the NCs is calculated. The d-band center of the cuboctahedral and octahedral NCs are -2.50 and -2.61, respectively. It has been previously reported that the expansion in the lattice parameters (under tensile strain) shifts the d-band center toward Fermi, which strengthens the binding strength of the adsorbate on the surface.[65-67] Interestingly, our calculations also show that the less compressive strained cuboctahedral NC shifts the d-band center toward Fermi and binds the reaction intermediates (*O and *OH) strongly. Therefore, the dissociation of $*O_2$ and formation of *OH become favorable on the cuboctahedral NC due to the stabilization of the products (*O and *OH).

Therefore, our detailed investigation concludes that the presence of small traces of (100) facet in the cuboctahedral NC induces compressive strain in the system, which in turn improves the activity; thus improves the adsorption of the intermediates (*O and *OH). As a result, cuboctahedral and octahedral NCs favour two different reaction mechanisms. Cuboctahedral NC prefers direct as well as indirect pathways for ORR mechanism. In contrary, octahedral NC favours indirect over direct pathway and thus increases the possibility of hydrogen peroxide formation (H_2O_2). Therefore we find that cuboctahedral NC improves the ORR activity and selectivity compared to the octahedral NC.

View Article Online
DOI: 10.1039/C6CY01709F

4. Kinetic Analysis

We have done a detailed kinetic analysis based on our preliminary DFT results to understand the product selectivity between four-electron (H_2O formation) vs. two-electron (H_2O_2 formation) reduction reactions. The forward (k_i) rate constants for all the elementary steps are calculated using the following equation:

$$k_i = \left(\frac{k_B T}{h}\right)\left(\frac{q_{TS}}{q_R}\right) e^{-\Delta G^{\ddagger}/k_B T}$$

where k_B is the Boltzmann constant, T is the temperature, h is the Plank constant. Here, q_{TS} and q_R are the vibrational partition functions for the transition state and reactant structures, respectively and $\Delta G^{\ddagger}$ is the Gibbs free energy barrier for the initial and final state of the elementary reaction. The vibrational partition functions (q) are calculated as follows

$$q = \sum_i \frac{1}{1 - e^{-h\nu_i/k_B T}}$$

where υ_i are the vibrational frequencies.

Table 3: Rate constants (s^{-1}) of the elementary reactions at different temperatures on the cuboctahedral NC (CNC) and octahedral NC (ONC). Here k_i stands for the forward rate constant of the i^{th} step.

Elementary reactions	300 K		400 K		500 K	
	CNC	ONC	CNC	ONC	CNC	ONC
$*O_2 \xrightarrow{k_1} *O+*O$	8.66×10^{12}	1.10×10^{10}	1.05×10^{13}	7.19×10^{10}	1.24×10^{13}	2.34×10^{11}
$*O_2+*H \xrightarrow{k_2} *OOH$	1.36×10^{12}	1.61×10^{11}	2.71×10^{12}	5.47×10^{11}	4.31×10^{12}	1.20×10^{12}
$*O+*H \xrightarrow{k_3} *OH$	1.32×10^{08}	1.30×10^{-04}	2.09×10^{09}	2.42×10^{00}	1.15×10^{10}	9.27×10^{02}
$*OOH \xrightarrow{k_4} *O+*OH$	7.92×10^{12}	7.54×10^{12}	9.72×10^{12}	1.01×10^{13}	1.22×10^{13}	1.26×10^{13}
$*H+*OOH \xrightarrow{k_5} *H_2O_2$	5.39×10^{-07}	8.17×10^{05}	4.21×10^{-02}	5.98×10^{07}	3.82×10^{01}	8.27×10^{08}
$*H_2O_2 \xrightarrow{k_6} *OH +$	8.73×10^{11}	6.65×10^{12}	2.06×10^{12}	8.87×10^{12}	3.62×10^{12}	1.11×10^{13}

*OH						
$\overset{k_7}{*H+*OH \rightarrow *H_2O}$	1.67×10^{13}	1.65×10^{13}	1.84×10^{13}	1.80×10^{13}	2.06×10^{13}	1.99×10^{13}

The rate constants (Table 3) are calculated in the temperature range of 300 K to 500 K as the fuel cell operates in this temperate range.[68,69] The rate constants improve significantly as we increase the temperature. At 300 K, the ratios of rate constants (k_1/k_2) between $*O_2$ dissociation and $*O_2$ hydrogenation steps are 6.36 and 0.07 on the cuboctahedral and octahedral NCs, respectively. Hence, *O formation is favorable over *OOH formation ($*O_2 \rightarrow *O + *O$ and $*O_2 + *H \rightarrow *OOH$) on the cuboctahedral surface, whereas both the steps are very much competing on the octahedral surface. However, it is very important to understand whether the shape of the NC affects the *OOH dissociation ($*OOH \overset{k_4}{\rightarrow} *O + *OH$) and hydrogenation ($*OOH + *H \overset{k_5}{\rightarrow} *H_2O_2$) steps or not? We find that the ratios of rate constants (k_4/k_5) of these two steps are 1.46×10^{19} and 9.22×10^{06} for the cuboctahedral and octahedral NCs, respectively; implying that the *OOH dissociation is very much favorable over *OOH hydrogenation on the cuboctahedral NC surface. Therefore, even if the reaction proceeds through the *OOH intermediate, it will further dissociate into *O and *OH ($*OOH \rightarrow *O + *OH$) on the cuboctahedral NC surface. Hence, our kinetic analysis suggests that cuboctahedral NC is highly selective and efficient towards four-electron reduction (H_2O formation) over two-electron reduction (H_2O_2 formation) reaction. More importantly, the rate-determining step ($*O+*H \rightarrow *OH$) is no longer a rate determining step (Table 3) when the reaction is catalyzed by the cuboctahderal NC.

Interestingly, the superior catalytic activity of the cuboctahedral NC over octahedral NC has been reported earlier. Wu et al.[70] investigated a series of Pt_3Ni NCs with fraction of exposed (111) and (100) facets and reported that the truncated-octahedral or cuboctahedral NCs with

View Article Online
DOI: 10.1039/C6CY01709F

highly exposed (111) facets increase the ORR mass activity by 1.8 times than that of the octahedral NCs. Carlos et al.[20] also concluded that the hexagonal Pt nanoparticle with (100) and (111) exposed facets displays the highest ORR activity in relative to the sphere (no preferential facets), tetrahedral/octahedral with (111) facets and cubic with (100) facets. Furthermore, the cuboctahedral NCs show better catalytic activity toward other reactions too. Gillian et al.[71] reported that the cuboctahedral palladium NC shows superior catalytic activity compared to the octahedral NC for Suzuki-Miyaura cross coupling reactions, where they attributed the presence of the (100) facet for showing better catalytic activity. Recently, Xia and co-workers[72] investigated the formic acid oxidation on different Pd polyhedrons enclosed by different proportion of (100) and (111) facets and concluded that the Pd nanocubes with slight 'truncations' at the corners to be the best catalysts. Wang et al.[73] reported that a 7 nm platinum nanoparticle consisting of (111) and (200) facets or only (100) facet transfers nearly four-electron (3.6) during ORR, whereas 3 and 5 nm nanoparticles with majorly (111) facet transfer less electron (0.7). Our calculation also shows that cuboctahedral NC favours four-electron reduction, whereas octahedral NC favours two-electron reduction. Moreover, Kim et al.[74] reported that octahedral Pd nanoparticles favour higher H_2O_2 selectivity during ORR, which is consistent with our results. However, many experimental reports conclude that cuboctahedral NC shows higher ORR activity while compared to octahedral NC. Therefore, the overall ORR activity of the NC is in good agreement with previous experimental reports.[20,70-74] Therefore, it is believed that the presence of the (100) facets along with the (111) facets (i.e. cuboctahedral, truncated-octahedral and hexagonal shape) shows superior catalytic activity than the purely (111) and (100) faceted NCs (i.e. octahedral and cubic shapes). Interestingly, our results are very much in consistent with previous experimental findings and this could be again due to the presence of two types of facets in the cuboctahedral NC. Therefore, our study not only provides an in-depth understanding behind

the shape-dependent catalytic activity but also illustrates the experimental finding in the atomic level.

5. Conclusion:

First-principle calculations are performed to understand the shape-dependent catalytic activities of the platinum NCs toward ORR activity. The cuboctahedral and octahedral platinum NCs enclosed by well-defined facets have been chosen for our study due to their high symmetry and experimental realization. Molecular dynamics simulation suggests that cuboctahedral NC is thermally more stable than octahedral NC and the cuboctahedral NC can withstand temperatures as high as 500 K without any structural reconstruction. Dissolution potential behaviors of the NCs show that cuboctahedral NC is electrochemically stable compared to the octahedral one. Reaction free energies and activation barriers are calculated for all the possible elementary steps of ORR on the (111) facet of the NCs. Our results reveal that the direct O-O bond dissociation is thermodynamically favorable over the NCs surface, which is totally opposite to previous theoretical on the bulk metal (Pt, Pd, Ag) surfaces, where indirect O-O bond dissociation is favorable over direct O-O bond dissociation. Furthermore, the rate-determining step is no longer a rate-determining step when the reaction is catalyzed by the cuboctahedral NC. Our kinetics analysis shows that the four-electron reduction (H_2O formation) is very favorable than the two-electron reduction (H_2O_2 formation) when the NCs. Hence, the efficiency and product selectivity (H_2O vs. H_2O_2) increased significantly when the reaction is catalyzed by the NCs. However, the efficiency and product selectivity reach maximum when the reaction is catalyzed by the cuboctahedral NC. After a detailed investigation on the surface energy and compressive strain, we find that, due to the presence of (111) and (100) facets, the cuboctahedral NC shifts the d-band center

View Article Online
DOI: 10.1039/C6CY01709F

position toward Fermi, which allows the NC to interact strongly with the intermediates, which in turn stabilizes the intermediates. As a result, cuboctahedral and octahedral NCs favour two different reaction mechanisms. Cuboctahedral NC prefers direct as well as indirect pathways for ORR mechanism. In contrary, octahedral NC favours indirect over direct pathway and thus increases the possibility of hydrogen peroxide formation (H_2O_2). Therefore we find that cuboctahedral NC improves the ORR activity and selectivity compared to the octahedral NC. Interestingly, earlier experimental reports show that the presence of (100) facets along with the (111) facets (i.e. cuboctahedral, truncated-octahedral and hexagonal NCs) shows superior catalytic activity than the purely (111) and (100) faceted NCs (i.e octahedral and cube shape), which is in well agreement with our findings. Therefore, our study provides atomistic insights into the shape-dependent catalytic activity of the platinum NCs toward ORR. We believe that our study will certainly help the experimentalists to understand the shape dependent catalytic activity of the NCs, which in turn will guide them for designing more efficient and selective catalyst for fuel cell applications.

Supporting Information:

Snapshots of the NCs after the simulation, a detailed discussion of the adsorption behaviors of the intermediates, derivation for the electrode potential shift during Pt dissolution, and calculation of surface energy, strain energy and percentage of strain have been given in Supporting Information.

Acknowledgments

We thank IIT Indore for the lab and computing facilities. This work is financially supported by DST-SERB.

References

[1] Y. Jiao, Y. Zheng, M. Jaroniecb and S. Z. Qiao, *Chem. Soc. Rev.* 2015, **44**, 2060.

[2] B. P. Vinayan, R. Nagar, N. Rajalakshmi, and S. Ramaprabhu, *Adv. Funct. Mater.* 2012, **22**, 3519.

[3] W. Lubitz, and W. Tumas, *Chem. Rev.* 2007, **107**, 3900.

[4] F. A. de Bruijn, V. A. T. Dam, and G. J. M. Janssen, *Fuel Cells* 2008, **8**, 3.

[5] M. Watanabe, D. A. Tryk, M. Wakisaka, H. Yano, and H. Uchida, *Electrochim. Acta* 2012, **84**, 187.

[6] F. Calle-Vallejo, M. T. M. Koper, and A. S. Bandarenka, *Chem. Soc. Rev.* 2013, **42**, 5210.

[7] X. X. Wang, Z. H. Tan, M. Zeng, and J. N. Wang, *Sci. Rep.* 2014, **4**, 4437.

[8] Y. Xu, A. V. Ruban, and M. Mavrikakis, *J. Am. Chem. Soc.* 2004, **126**, 4717.

[9] V. R. Stamenkovic, B. Fowler, B. S. Mun, G. Wang, P. N. Ross, C. A. Lucas, and N. M. Marković, *Science* 2007, **315**, 493.

[10] V. Stamenkovic, B. S. Mun, K. J. J. Mayrhofer, P. N. Ross, N. M. Markovic, J. Rossmeisl, J. Greeley, and J. K. Nørskov, *Angew. Chem.* 2006, **118**, 2963.

[11] W. J. Tang, L. Zhang, and G. Henkelman, *J. Phys. Chem. Lett*. **2011**, *2*, 1328−1331.

[12] A. Holewinski, J. Idrobo, and S. Linic, *Nat. Chem.*2014, **6**, 828–834.

[13] J. X. Wang, H. Inada, L. Wu, Y. Zhu, Y. Choi, P. Liu, W. P. Zhou, and R. R. Adzic, *J. Am. Chem. Soc.* 2009, **131**, 17298.

[14] M. Oezaslan, F. Hasché, and P. Strasser, *J. Phys. Chem. Lett.* 2013, **4**, 3273.

[15] V. Mazumder, M. Chi, K. L. More, and S. Sun, *J. Am. Chem. Soc.* 2010, **132**, 7848.

[16] L. D. Pachon, and G. Rothenberg, *App. Organometal. Chem.* 2008, **22**, 288.

[17] Y. Wang, N. Zhao, B. Fang, H. Li, X. T. Bi, and H. Wang, *Chem. Rev*. 2015, **115**, 3433.

[18] T. S. Ahmadi, Z. L. Wang, T. C. Green, A. Henglein, and M. A. El-Sayed, *Science.* 1996, **272**, 1924.

[19] C. Wang, H. Daimon, T. Onodera, T. Koda, S. Sun, *Angew. Chem. Int. Ed.* 2008, **47**, 3588.

[20] C. M. Sanchez, J. Solla-Gullon, F. J. Vidal-Iglesias, A. Aldaz, V. Montiel, and E. Herrero, *J. Am. Chem. Soc.* 2010, **132**, 5622.

[21] J. Zhang, H. Yang, J. Fang, and S. Zou, *Nano Lett.* 2010, **10**, 638.

[22] B. Lim, M. Jiang, J. Tao, P. H. C. Camargo, Y. Zhu, and Y. Xia, *Adv. Funct. Mater.* 2009, **19**, 189.

[23] B. Y. Xia, H. B. Wu, X. Wang, and X. W. Lou, *Angew. Chem. Int. Ed.* 2013, **52**, 12337.

[24] Y. Tang, and W. Cheng, *Langmuir* 2013, **29**, 3125.

[25] B. R. Cuenya, *Acc. Chem. Res.* 2013, **46**, 1682.

[26] Wu, J., and H. Yang, *Acc. Chem. Res.* 2013, **46**, 1848.

[27] Y. Tang, and W. Cheng, *Nanoscale*, 2015, **7**, 16151.

[28] F. Vines, J. R. B. Gomes, and F. Illas, *Chem. Soc. Rev*. 2014, **43**, 4922.

[29] R. Narayanan, and M. A. El-Sayed, *J. Phys. Chem. B.* 2005, **109**, 12663.

[30] K.M. Bratlie, H. Lee, K. Komvopoulos, P. Yang, G.A. Somorjai, *Nano Lett*. 2007, **7**, *3097*.

[31] C. K. Tsung, , J. N. Kuhn, W. Huang, C. Aliaga, L. I. Hung, G. A. Somorjai, P. Yang, *J. Am. Chem.Soc.* 2009, **131**, 5816.

[32] I. Lee, F. Delbecq, R. Morales, M.A. Albiter, and F. Zaera, *Nat.Mater*. 2009, **8**, 132.

[33] J. Wang, J. Gong, Y. Xiong, J. Yang, Y. Gao, Y. Liu, X. Lu, and Z. Tang, *Chem. Commun*, 2011, **4***7*, 6894.

[34] X. Zhang, H. Yin, J. Wang, L Chang, Y. Gao, W. Liu, and Z. Tang, *Nanoscale*. 2013, **5**, 8392.

[35] R. Wang, H. He, L.-C. Liu, H.-X. Dai, and Z. Zhao, *Catal.Sci.Technol.* 2012, **2**, 575.

[36] Y. Nie, L. Li, and Z. Wei, *Chem. Soc. Rev.* 2015, **44**, 2168.

[37] A. Rabis, P. Rodriguez, T. J. Schmidt, *ACS Catal.* 2012, **2**, 864.

[38] (a) Y. Hu, H. Zhang, P. Wu, H. Zhang, B. Zhou, C. Cai, *Phys. Chem. Chem. Phys.* 2011, **13**, 4083. (b) T. Maiyalagan, and F. N. Khan, *Catal. Commun.* 2009, **10**, 433.

[39] E. Yeager, *J. Mol. Catal.* 1986, **38**, 5.

[40] C. M. Sanchez-Sanchez, and A. Bard, J. *Anal. Chem.* 2009, **81**, 8094.

[41] (a) Markovic, N. M.; Gasteiger, H. A.; Ross, P. N. *J. Phys. Chem*. 1996, **100**, 6715. (b) Tian, N.; Zhou, Z. Y.; Sun, S. G.; Ding, Y.; Wang, Z. L. *Science*, 2007, **316**, 732. (c) Susut, C.; Chapman, G. B.; Samjeske, G.; Osawa, M.; Tong, Y. Y. J. *Phys. Chem. Chem. Phys.*, 2008, **10**, 3712. (d) Solla-Gullon, J.; Vidal-Iglesias, F. J.; Lopez-Cudero, A.; Garnier, E.; Feliu, J. M.; Aldaz, A. *Phys. Chem. Chem. Phys*., 2008, **10**, 3689. (e) Duan, Z.; Wang, G. *J.*

Phys. Chem. C 2013, **117**, 6284. (f) Han, B.; Viswanathan, V.; Pitsch, H. *J. Phys. Chem. C* 2012, **116**, 6174. (g) A. Mahata, K. S. Rawat, I. Choudhuri, B. Pathak, *J. Mater. Chem. A,* 2016, **4**, 12756. (h) A. Mahata, K. S. Rawat, I. Choudhuri, B. Pathak, *Scientific Reports* 2016, **6**, 25590.

[42] P. E. Blochl, *Phy. Rev. B* 1994, **50**, 17953.

[43] (a) G. Kresse, and J. Hafner, *Phy. Rev. B* 1993, **47**, 558. (b) G. Kresse, and J. Hafner, *Phy. Rev. B* 1994, **49**, 14251-14269. (c) G. Kresse, and D. Joubert, *Phy. Rev. B* 1999, **59**, 1758.

[44] J. P. Perdew, J. A. Chevary, S. H. Vosko, K. A. Jackson, M. R. Pederson, D. J. Singh, and C. Fiolhais, *Phy. Rev. B* 1992, **46**, 6671.

[45] S. Grimme, J. Antony, S. Ehrlich, and S. Krieg, *J. Chem. Phys.* 2010, **132**, 154104.

[46] Henkelman, G., Jonsson, H. *J. Chem. Phys.* **2000**, *113*, 9978-9985.

[47] Kittel, C. *Introduction to Solid State Physics,* 8th edition. Hoboken, NJ: John Wiley & Sons, Inc, **2005**.

[48] (a) I. Choudhuri, N. Patra, A. Mahata, R. Ahuja, and B. Pathak, *J. Phys. Chem. C* 2015, **119**, 24827. (b) P. Garg, S. Kumar, I. Choudhuri, A. Mahata, B. Pathak, *J. Phys. Chem. C*; 2016, **120**, 7052. (c) I. Choudhuri, S. Kumar, A. Mahata, K. Rawat, B. Pathak, *Nanoscale*; 2016, **8**, 14117.

[49] Z. Shi, Z. Zhang, A. Kutana, B. I. Yakobson, *ACS Nano*, 2015, **9**, 9802.

[50] S. A. Nose, *J. Chem. Phys.* 1984, **81**, 511-519.

[51] M. C. S. Escano, *Nano Res*. 2015, **8**, 1689.

[52] T. Jeon, S. Kim, N. Pinna, A. Sharma, J. Park, S. Lee, H. C. Lee, S. Kang, H. Lee, H. H. Lee *Chem. Mater*., 2016, **28**, 1879.

[53] Y. Ma, and P. B. Balbuena, *J. Phys. Chem. C* 2008**, 112***,* 14520.

[54] J. Greeley, and J. K. Nørskov, *Electrochimica Acta* 2007, **52***,* 5829.

[55] G. Caballero, P. B. Balbuena, *J. Phys. Chem. Lett.* **2010**, **1**, 724.

[56] H. Kikuchi, W. Ouchida, M. Nakamura, C. Goto, M. Yamada, H. Nagahiro. *Electrochem. Commun.* 2010. **12**,54.

[57] R. Devivaraprasad, T. Kar, A. Chakraborty, R. K. Singh, M. Neergat, *Phys. Chem. Chem. Phys.*, 2016, **18**, 11220.

[58] K. Li, Y. Li, Y. Wang, F. He, M. Jiao, H. Tang, and Z. Wu, *J. Mater. Chem. A* 2015, **3**, 11444.

[59] Y. Sha, T. H. Yu, B. V. Merinov, P. Shirvanian, W. A. Goddard, *J. Phys. Chem. Lett*. 2011, **2**, 572.

[60] C. A. Farberow, A. Godinez-Garcia, G. W. Peng, J. F. Perez-Robles, O. Solorza-Feria, and M. Mavrikakis, *ACS Catal.* 2013, **3**, 1622.

[61] P. C. Jennings, H. A. Aleksandrov, K. M. Neymanbd, and R. L. Johnston, *Nanoscale* 2014, **6**, 1153.

[62] Y. Sha, T. H. Yu, Y. Liu, B. V. Merinov, W. A. Goddard III, *J. Phys. Chem. Lett*. 2010, **1**, 856.

[63] Z. Duan, and G. Wang, *Phys. Chem. Chem. Phys.* 2011, **13**, 20178.

[64] (a) D. Gao, H. Zhou, J. Wang, S. Miao, F. Yang, G. Wang, J. Wang, X. Bao, *J. Am. Chem. Soc.* 2015, **137**, 4288. (b) Q. Cai, J. Wang, Y. Wang, D. Mei, *AIChE J.,* 2015, **61**, 3812. (c) J. Lyu, J. Wang, C. Lu, L. Ma, Q. Zhang, X. He, X. Li, *J. Phys. Chem. C* 2014, **118**, 2594.

[65] M. Mavrikakis, B. Hammer, and J. K. Nørskov, *Phys. Rev. Lett.* 1998, **81**, 2819.

[66] J. R. Kitchin, J. K. Nørskov, M. A. Barteau, and J. G. Chen, *Phys. Rev. Lett.* 2004, **93**, 156801.

[67] S. Kattel, and G. Wang, *J. Chem. Phys.* 2014, **141**, 124713.

[68] A. Mahata, I. Choudhuri, and B. Pathak, *Nanoscale* 2015, **7**, 13438.

[69] V. Mehta, and J. S. Cooper, *J. Power Sources* 2003**, 114**, 32.

[70] J. Wu, J. Zhang, Z. Peng, Yang, S., F. T. Wagner, and H. Yang, *J. Am. Chem. Soc.* 2010, **132**, 4984.

[71] G. Collins, M. Schmidt, C. Dwyer, J. D. Holmes, and G. P. McGlacken, *Angew. Chem. Int. Ed.* 2014, **53**, 4142.

[72] M. Jin, H. Zhang, Z. Xieb, and Y. Xia, *Energy Environ. Sci.* 2012, **5**, 6352.

[73] C. Wang, H. Daimon, T. Onodera, T. Koda, and S. Sun, *Angew. Chem. Int. Ed.* 2008, **47**, 3588.

[74] S. Kim, D. Lee, K. Lee, *J. Mol. Cat. A: Chemical* 2014, **391**, 48.

Table of Content

View Article Online
DOI: 10.1039/C6CY01709F